

See discussions, stats, and author profiles for this publication at: <https://www.researchgate.net/publication/51044750>

High-Pressure Study of Lithium Azide from Density-Functional Calculations

ARTICLE *in* THE JOURNAL OF PHYSICAL CHEMISTRY A · MAY 2011

Impact Factor: 2.69 · DOI: 10.1021/jp200907q · Source: PubMed

CITATIONS

15

READS

68

4 AUTHORS, INCLUDING:



Bheema Lingam Chittari

University of Seoul

22 PUBLICATIONS 113 CITATIONS

[SEE PROFILE](#)



Surya Tewari

University of Hyderabad

178 PUBLICATIONS 1,325 CITATIONS

[SEE PROFILE](#)



Ganapathy Vaitheswaran

University of Hyderabad

118 PUBLICATIONS 1,343 CITATIONS

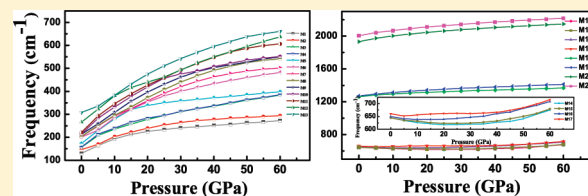
[SEE PROFILE](#)

High-Pressure Study of Lithium Azide from Density-Functional Calculations

K. Ramesh Babu,[†] Ch. Bheema Lingam,[‡] Surya P. Tewari,^{†,‡} and G. Vaitheswaran^{*,†}

[†]Advanced Centre of Research in High Energy Materials (ACRHEM) and [‡]School of Physics, University of Hyderabad, Prof. C. R. Rao Road, Gachibowli, Andhra Pradesh, Hyderabad 500 046, India

ABSTRACT: The structural, electronic, optical, and vibrational properties of LiN_3 under high pressure have been studied using plane wave pseudopotentials within the generalized gradient approximation for the exchange and correlation functional. The calculated lattice parameters agree quite well with experiments. The calculated bulk modulus value is found to be 23.23 GPa, which is in good agreement with the experimental value of 20.5 GPa. Our calculations reproduce well the trends in high-pressure behavior of the structural parameters. The present results show that the compressibility of LiN_3 crystal is anisotropic and the crystallographic *b*-axis is more compressible when compared to *a*- and *c*-axes, which is also consistent with experiment. Elastic constants are predicted, which still awaits experimental confirmation. The computed elastic constants clearly show that LiN_3 is a mechanically stable system and the calculated elastic constants follow the order $C_{33} > C_{11} > C_{22}$, implying that the LiN_3 lattice is stiffer along the *c*-axis and relatively weaker along the *b*-axis. Under the application of pressure the magnitude of the electronic band gap value decreases, indicating that the system has the tendency to become semiconductor at high pressures. The optical properties such as refractive index, absorption spectra, and photoconductivity along the three crystallographic directions have been calculated at ambient as well as at high pressures. The calculated refractive index shows that the system is optically anisotropic and the anisotropy increases with an increase in pressure. The observed peaks in the absorption and photoconductivity spectra are found to shift toward the higher energy region as pressure increases, which implies that in LiN_3 decomposition is favored under pressure with the action of light. The vibrational frequencies for the internal and lattice modes of LiN_3 at ambient conditions as well as at high pressures are calculated from which we predict that the response of the lattice modes toward pressure is relatively high when compared to the internal modes of the azide ion.



I. INTRODUCTION

Alkali metal azides are an interesting class of compounds which find a wide range of applications as explosives and photographic materials. These are model systems for studying the fast reactions in solids with complex chemical bonding.^{1,2} Under the action of heat and light, these metal azides become unstable and decompose into metal and nitrogen. Since the decomposition of metal azides involves the electron-transfer mechanism, it would be necessary to understand the electronic band structure of these systems.³ A number of studies at the level of Hartree–Fock (HF) and density functional theory (DFT) has been performed to understand the electronic band structure and decomposition mechanism.^{4–8} Moreover, the high-pressure behavior of metal azides is an important aspect because of the formation of polymeric nitrogen, a high energy density material.^{9,10} Previously the high-pressure study on sodium azide, NaN_3 , revealed that a new structure is formed with nitrogen atoms connected by single covalent bonds, which was considered to be an amorphous-like structure.¹¹ Since NaN_3 and LiN_3 are isostructural at ambient conditions, it would be of interest to study the pressure effect on LiN_3 with the motive of formation of polymeric nitrogen. Recently Medvedev et al.¹² reported the behavior of LiN_3 under high pressures. Their study revealed that the system is stable up to the pressure of 60 GPa, which is in

contrast to that of sodium azide which undergoes a set of phase transitions below the pressures of 50 GPa.¹² With this motivation we aim to study theoretically the pressure effect on the LiN_3 crystal system. To understand the behavior of LiN_3 under high pressure, it is essential to study the physical and chemical properties of the system under high pressure. To the best of our knowledge the structural, electronic, vibrational, and optical properties of LiN_3 at high pressures have not been explored theoretically. Moreover, these properties under pressure are important in a better understanding of the stability of LiN_3 . In this paper, we present a first-principles study of solid monoclinic LiN_3 under hydrostatic pressure of up to 60 GPa using density functional theory. The structural parameters, bulk modulus, energy band gap, density of states, optical and vibrational properties of LiN_3 under pressure are reported. The remainder of the paper is organized as follows: A brief description of our computational method is given in section II. The results and discussion are presented in section III. Finally we end with a brief summary of our conclusions in section IV.

Received: January 27, 2011

Revised: March 14, 2011

Published: April 12, 2011

II. COMPUTATIONAL DETAILS

The first-principles density functional theory calculations were performed with the Cambridge Sequential Total Energy package program,^{13,14} using Vanderbilt-type ultrasoft pseudopotentials¹⁵ and a plane wave expansion of the wave functions. The electronic wave functions were obtained using a density mixing scheme,¹⁶ and the structures were relaxed using the Broyden, Fletcher, Goldfarb, and Shannon (BFGS) method.¹⁷ The exchange-correlation potential of Ceperley and Alder¹⁸ parametrized by Perdew and Zunger¹⁹ in the local density approximation (LDA) and also the generalized gradient approximation (GGA) with the Perdew–Burke–Ernzerhof (PBE) parametrization²⁰ were used to describe the exchange-correlation potential. The pseudoatomic calculations were performed for Li 2s¹ and N 2s²2p³. The Monkhorst–Pack scheme *k*-point sampling was used for integration over the Brillouin zone.²¹ The convergence criteria for structure optimization and energy calculation were set to ultrafine quality. It is well-known that the cutoff energy and *k*-point mesh influence the convergence of calculations; we tested the dependence of energy cutoff and the *k*-point grid and found that for the 520 eV plane wave cutoff energy and 5 × 8 × 5 *k*-point mesh, the change in total energy is less than 1 meV. So we chose this plane wave cutoff energy and *k*-point mesh for all the calculations.

We performed the calculation by adopting the experimental crystal structure,²² $a = 5.627 \text{ \AA}$, $b = 3.319 \text{ \AA}$, $c = 4.979 \text{ \AA}$, and $\beta = 107.4^\circ$ as the initial structure, and it is relaxed to allow the ionic configurations, cell shape, and volume to change at ambient pressure. Our calculations were conducted on one unit cell with two molecules. Starting from the optimized crystal structure of lithium azide at ambient pressure, we applied hydrostatic pressure up to 60 GPa. The external pressure was gradually increased by an increment of 1 GPa in each time. Under a given pressure, the internal coordinates and unit cell parameters of the lithium azide crystal were determined by minimizing the Hellmann–Feynmann force on the atoms and the stress on the unit cell simultaneously. In the geometry relaxation, the self-consistent convergence on the total energy is $5 \times 10^{-7} \text{ eV/atom}$ and the maximum force on the atom is found to be 10^{-4} eV/\AA . On the basis of the equilibrium structures, the electronic, optical, and vibrational properties have been calculated. The vibrational frequencies have been calculated from the response to small atomic displacements.^{23,24} The elastic constants are calculated for the optimized crystal structure at ambient conditions by using volume-conserving strain technique²⁵ as implemented in the CASTEP code. We have relaxed the internal coordinates of the strained unit cell to arrive at the elastic constants.

III. RESULTS AND DISCUSSION

A. Crystal Structure and Properties at Ambient Pressure.

At ambient pressure, LiN₃ crystallizes in the monoclinic structure with the *C*2/*m* space group and contains two molecules per unit cell. Each azide ion is surrounded by six cations and vice versa. The structure is isostructural to the low-temperature phase of sodium azide (α NaN₃). To determine the theoretical equilibrium crystal structure for lithium azide, we performed a full geometry optimization of both the lattice constants and the internal atomic coordinates within LDA and GGA. The crystal structure of LiN₃ from our geometry optimization in GGA is shown in Figure 1. In Table 1, we compare the lattice constants and unit cell volume with experimental data²² and previous

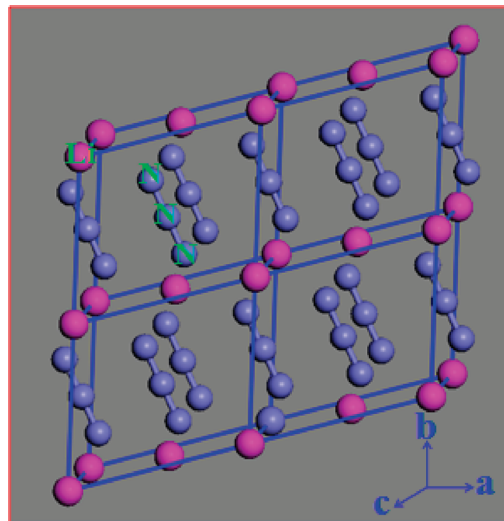


Figure 1. Crystal structure of LiN₃.

theoretical results.^{8,26} Compared to the experimentally measured lattice constants of LiN₃, our LDA calculations underestimate *a*, *b*, and *c* by 5.3, 3.6, and 5.1%, whereas GGA calculations overestimate *a*–*c* by 2.3, 1.7, and 2.3%, respectively. This discrepancy between theory and experiment can be expected for a molecular crystal such as LiN₃ where the van der Waals forces are important, which could not be dealt with the LDA and GGA in the DFT calculations.²⁷ However, our calculated volume of LiN₃ using GGA is closer (less error) to the experimental volume when compared to LDA, and therefore for further calculations we adopted GGA.

B. Structural and Electronic Properties under Pressure.

Starting from the zero-pressure equilibrium lattice structure, we applied hydrostatic compression to the LiN₃ unit cell in the pressure range from 0 to 60 GPa. This was done through CASTEP using variable cell optimization under the constraint of a diagonal stress tensor with fixed values of diagonal matrix elements equal to a desirable pressure. The obtained pressure–volume relation of LiN₃ is shown in Figure 2a, together with the results of experiment by Medvedev et al.¹² Our calculations show that the volume decreases monotonically with pressure and at 60 GPa the volume compression is $V/V_0 = 57\%$. Qualitatively our calculations reproduce the trend of pressure-induced reduction of volume by experiment (where the volume compression at 62 GPa is $V/V_0 = 58\%$). From the calculated *P*–*V* relation we can also observe that, at a given pressure, the theoretical unit cell volume is greater than that of the experiment, which is also due to the inherent limitation of DFT-GGA functionals. However, as pressure increases, the computed cell volume approaches the experimental values. For example, if we observe keenly, the discrepancy between theoretical and experimental volumes decreases from 5.8% at 0 GPa to 2.68% at 60 GPa. This result implies that our ab initio-GGA calculations performed under high pressure might be more reliable.

The dependence of lattice constants of LiN₃ on pressure is shown in Figure 2b, where our theoretical results are compared with the experimental data.¹² The experimental trend for the lattice constants upon compression is well-reproduced by our GGA calculations. Among the three axes, we find the better agreement between our GGA calculations and experiments for reduction of lattice constant for the *b*-axis, whereas the

Table 1. Calculated Ground-State Properties of Monoclinic LiN₃ at Ambient Pressure

lattice parameter	present work		other calculations	experiment ^c
	LDA	GGA		
<i>a</i> (Å)	5.328	5.761	5.696 ^a , 5.626 ^b	5.627
<i>b</i> (Å)	3.199	3.376	3.235 ^a , 3.317 ^b	3.319
<i>c</i> (Å)	4.727	5.094	5.263 ^a , 5.035 ^b	4.979
β , deg	102.62	108.6	113.5 ^a , 106.7 ^b	107.4
Li	(0, 0, 0)	(0, 0, 0)	(0, 0, 0) ^b	(0, 0, 0)
N	(0.1244, 0.5, 0.7456)	(0.1005, 0.5, 0.7490)	(0.1040, 0.5, 0.7376) ^b	(0.1048, 0.5, 0.7397)
N	(0, 0.5, 0.5)	(0, 0.5, 0.5)	(0, 0.5, 0.5) ^b	(0, 0.5, 0.5)
<i>B</i> ₀ (GPa)	42.27	23.23		20.5 ^d

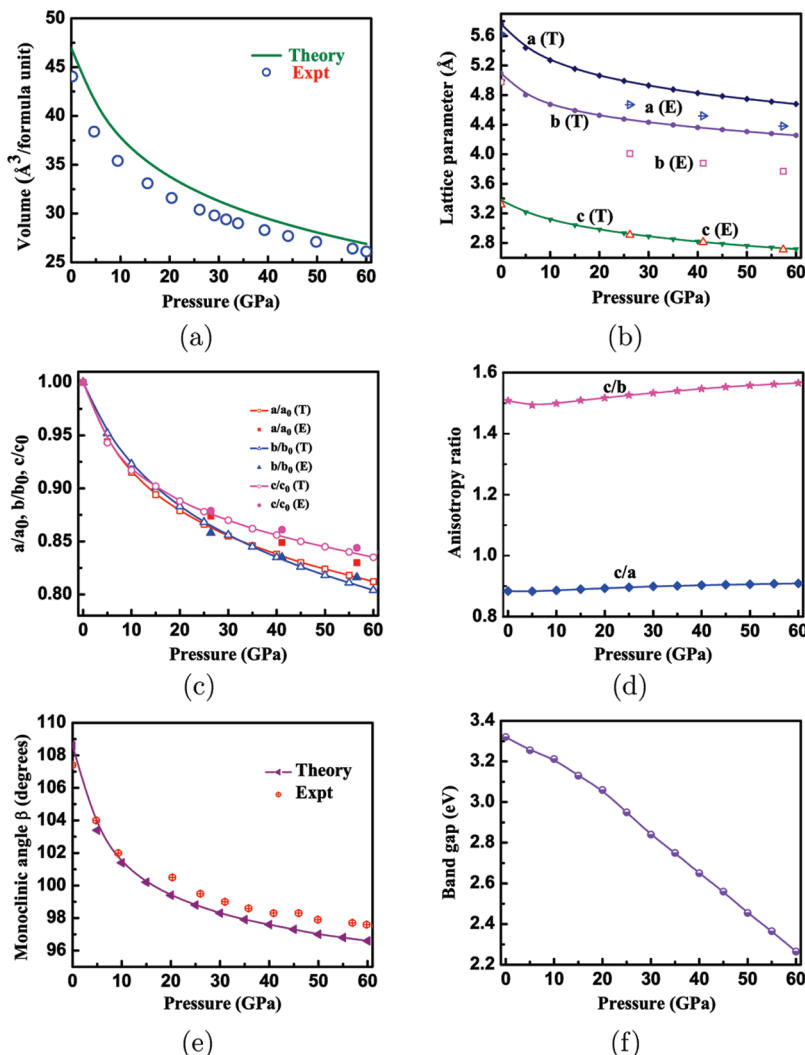
^a Reference 26. ^b Reference 8. ^c Reference 22. ^d Reference 12.

Figure 2. (a) Volume variation of LiN₃ with pressure, (b) variation of lattice parameters of LiN₃ with pressure, (c) variation of normalized lattice parameters of LiN₃ with pressure, (d) variation of *c/a* and *c/b* of LiN₃ with pressure, (e) variation of the monoclinic angle β of LiN₃ with pressure, and (f) band gap variation of LiN₃ with pressure.

reduction of the lattice constant for *a*- and *c*-axes is overestimated by our calculation. The possible reason for this behavior is the theoretical values of initial zero-pressure lattice constant; *a* and *c* are 2.3% larger than the experimental values (see Table 1).

In Figure 2c, we have shown the trends in the ratios of *a/a*₀, *b/b*₀, and *c/c*₀ of LiN₃ as a function of pressure along with the experimental data.¹² It can be observed that the *b*-axis is the most compressible which is also consistent with experimental

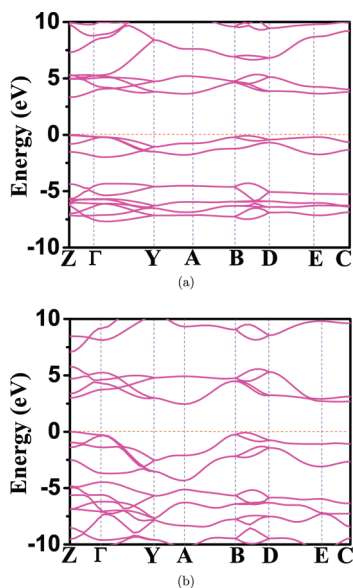


Figure 3. Band structure of LiN_3 (a) at 0 GPa and (b) at 60 GPa.

result. The anisotropy ratios c/a and c/b with increasing pressure are shown in Figure 2d. The c/a ratio increases from 0.884 at 0 GPa to 0.909 at 60 GPa, whereas the c/b ratio increases from 1.508 at 0 GPa to 1.566 at 60 GPa, which indicates that the compressibility of LiN_3 is anisotropic. This is in good agreement with the experiment.¹² The pressure dependence of the monoclinic angle of LiN_3 is shown in Figure 2e, where it is also compared with experiment.¹² The change in monoclinic angle is more below 20 GPa, whereas above this pressure it is only of 2° ; this implies that the shear of layers is more below 20 GPa, whereas it is less pronounced at high pressures (at 60 GPa). Due to the effect of the shear of the structure, the azide ions become closer to each other and therefore the interaction will be more.

The electronic structure of solids can be characterized by means of electronic band gap. The electronic band structure of LiN_3 at 0 GPa and at 60 GPa are shown in Figures 3a,b, respectively. The band structure at 0 GPa clearly shows that the top of the valence band and the bottom of the conduction band occurs at Z-point in the Brillouin zone, indicating that the material is a direct band gap material with a separation of 3.32 eV, the value slightly lower than the previous theoretical value of 3.46 at the PWGGA-DZP level²⁶ and 3.7 eV in ref 6. Unfortunately, as far as we know, there is no experimental value of the band gap available for LiN_3 to compare our theoretical band gap result. Of course, we could expect that our band gap value might be lower than the experimental band gap, because it is well-known that first-principles calculation of the electronic structure of semiconductors and insulators using GGA gives an underestimation of the band gap values compared to experiments.^{28–30} This underestimation of the gap is mainly due to the fact that GGA suffers from artificial electron self-interaction and also lacks the derivative discontinuities of the exchange-correlation potential with respect to occupation number. One way to solve the band gap problem is to apply a perturbative correction to the energy levels, as in the GW approximation.^{31,32} However the band gap at 60 GPa is observed to be indirect as it occurred between the Z- and A-points. On the basis of the equilibrium crystal structures obtained at different pressures, we calculated the band gap and examined its change under hydrostatic compression. The

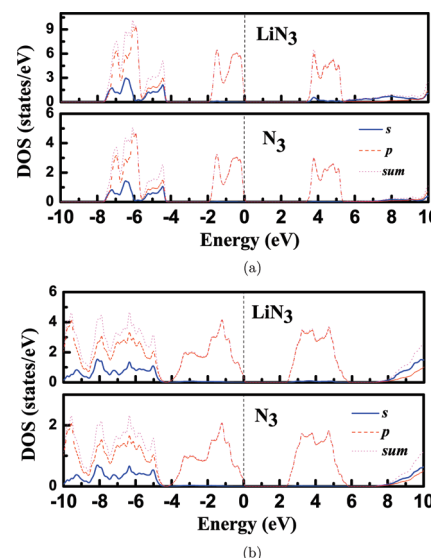


Figure 4. Total and partial DOS of LiN_3 (a) at 0 GPa and (b) at 60 GPa.

calculated band gaps as functions of pressure are shown in Figure 2f. It can be seen that the band gap reduces smoothly under compression without any significant discontinuity. But in different pressure ranges the average decrease of the band gap is different (up to 20 GPa 0.065 eV/GPa and 0.1 eV/GPa from 20 to 60 GPa). The decrease in the band gap with pressure indicates that the electrical conductivity of LiN_3 increases, meaning that at high pressures LiN_3 might change from insulator to semiconductor.

The nature of bonding and the electronic band gap under pressure can be studied by the total and partial DOS. Moreover, lithium azide is photosensitive and undergoes decomposition under the action of a suitable wavelength of light, and the essential step in the photochemical decomposition involves the promotion of a valence electron from the valence band to the conduction band; therefore, it would be necessary to know the information about the type of states that are present in both valence and conduction bands. For LiN_3 , the total and partial DOS at ambient and at 60 GPa pressure are shown in Figure 4a,b, respectively. Overall the distribution of states is the same at both pressures, and there is no hybridization between the Li states and N_3 states at ambient pressure as well as at 60 GPa, indicating that the ionic bond is more favored in LiN_3 . This is also observed by using the charge density distribution plots shown in Figure 5a,b. The p states of azide ion are dominating at the Fermi level, and as pressure increases the delocalization of the azide ion states is observed; see Figure 4b. This is also clearly observed by the charge density distribution plots shown in Figure 5c,d. We have also shown the charge density plots of the states at the minimum of the conduction band which are also derived mostly from the p type azide states and very little contribution from the s states of Li and azide ion both at 0 and 60 GPa in Figure 5e,f, respectively.

C. Bulk Modulus and Elastic Constants. To know about the crystal stiffness and the mechanical stability at ambient conditions, we calculated the bulk modulus and elastic constants of LiN_3 . The calculated values are listed in Table 2 (bulk modulus value is shown in Table 1). Our calculated bulk modulus value within GGA is 23.23 GPa, and it is slightly overestimated by that of the reported value of 20.5 by Medvedev et al.,¹² but it is still comparable with that of alkali halide crystal NaCl for which $B = 23.84$ GPa. We have also given the calculated LDA bulk

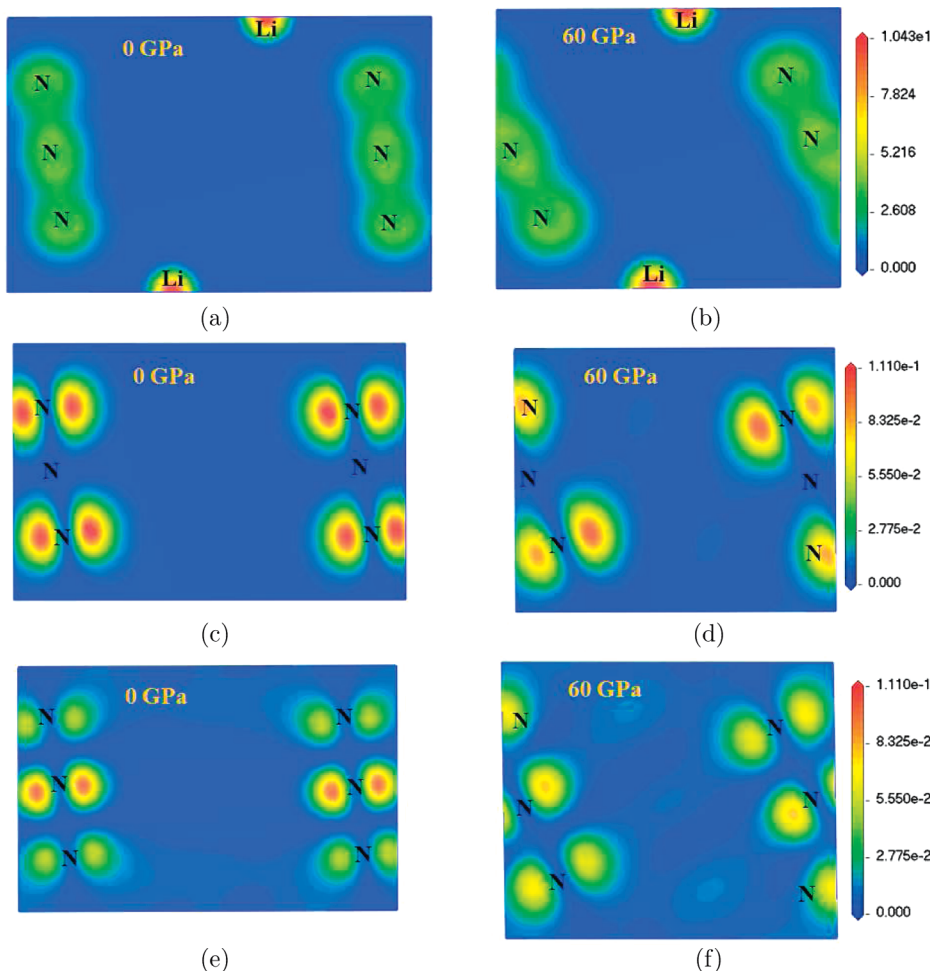


Figure 5. Charge density distribution of LiN_3 at 0 GPa (a) and at 60 GPa (b) (where, for example, $1.043\text{e}1$ represents 1.043×10). Panels c and d are of the states near by the Fermi level, and e and f are of the minimum of the conduction band.

modulus value for comparison. One should note here that our LDA bulk modulus value is overestimated by that of the GGA value and the experiment. This might be due to the fact that LDA overbinds the system as the volume is largely underestimated, which is a common feature in DFT-LDA calculations, and therefore one would expect large bulk modulus. Since the bulk modulus values are different in LDA and GGA, therefore the choice of exchange-correlation functional is also very important for this system. Our GGA bulk modulus value is in good agreement with that of experiment; this once again shows that the GGA functional is the good exchange-correlation functional for this system. As expected for ionic solids, lithium azide is a soft material because of its low bulk modulus value. For a monoclinic crystal there are 13 independent elastic constants, namely, C_{11} , C_{22} , C_{33} , C_{44} , C_{55} , C_{66} , C_{12} , C_{13} , C_{15} , C_{23} , C_{25} , C_{35} , and C_{46} . The mechanical stability of the crystal requires that the whole set of elastic constants satisfies the Born–Huang criterion.³³ For the case of LiN_3 , it is found that the calculated elastic constants obey this stability criteria and therefore the monoclinic lithium azide is mechanically a stable compound. Furthermore for a molecular crystal such as LiN_3 one can correlate the elastic constant values with the structural properties of the crystal. Since LiN_3 is a monoclinic system, the elastic constants C_{11} , C_{22} , and C_{33} can be directly related to the crystallographic *a*-, *b*-, and *c*-axes,

Table 2. Single-Crystal Elastic Constants (C_{ij} , GPa) of LiN_3 Calculated at the Theoretical Equilibrium Volume

parameter	parameter	parameter			
C_{11}	56.1	C_{66}	15.2	C_{25}	2.6
C_{22}	48.1	C_{12}	19.6	C_{35}	41.1
C_{33}	102.9	C_{13}	27.9	C_{46}	-1.7
C_{44}	9.6	C_{15}	6.1		
C_{55}	26.7	C_{23}	19.5		

respectively. The calculated values of these three constants follow the order $C_{33} > C_{11} > C_{22}$, which implies that the elastic constant C_{22} is the weakest for LiN_3 . This reveals the fact that a relative weakness of lattice interactions is present along the crystallographic “*b*”-axis. For the relative magnitude of the elastic constants C_{11} and C_{33} the analysis of the crystal structure of LiN_3 shows that the largest number of close-contact (less than 2.3 Å) intermolecular interactions to be situated along the crystallographic *c*-axis. Therefore the increased number of interactions along the *c*-axis would stiffen the lattice in this direction, which is consistent with the value of C_{33} . The lowest number of interactions is along the *b*-axis, which is further supported by the lowest value of C_{22} .

D. Optical Properties under High Pressure. Lithium azide becomes unstable and undergoes decomposition by the action of

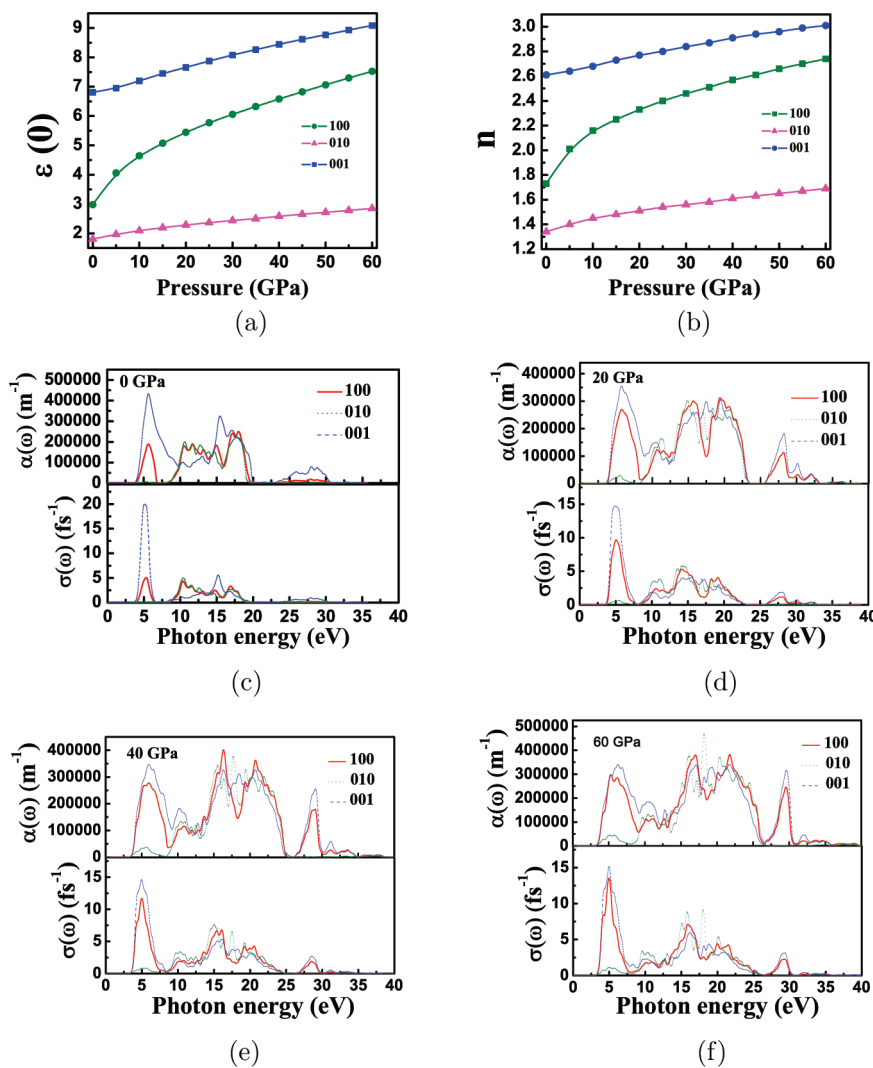
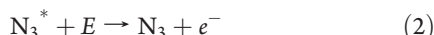


Figure 6. (a) Calculated static dielectric constant as a function of pressure, (b) calculated refractive index of LiN_3 as a function of pressure, and calculated absorption and photoconductivity of LiN_3 at the pressures of (c) 0, (d) 20, (e) 40, and (f) at 60 GPa.

light. The photochemical decomposition of lithium azide can be understood by the optical transitions from the valence band to the conduction band. From the total and partial DOS the states lying near the Fermi level are the p states of azide ion; therefore the decomposition of the lithium azide can be initiated by the formation of azide radicals in the following way.



where E is the thermal energy required to dissociate the azide radical N_3^* . The combination of two positive holes will give nitrogen gas with the liberation of energy Q and the electron trapped to the metal atom sites and thereby form the metal atom



Therefore, to understand the photochemical decomposition phenomena at ambient as well as at high pressures, it would be necessary to understand its optical properties that are resulting from the

interband transitions. In general the optical properties of matter can be described by means of the complex dielectric function $\epsilon(\omega) = \epsilon_1(\omega) + i\epsilon_2(\omega)$, where $\epsilon_1(\omega)$ and $\epsilon_2(\omega)$ describe the dispersive and absorptive parts of the dielectric function. Normally there are two contributions to $\epsilon(\omega)$, namely, intraband and interband transitions. The contribution from intraband transitions is important only for the case of metals. The interband transitions can further be split into direct and indirect transitions. The indirect interband transitions involve scattering of phonons. But the indirect transitions give only a small contribution to $\epsilon(\omega)$ in comparison to the direct transitions, so we neglected them in our calculations. The direct interband contribution to the absorptive or imaginary part $\epsilon_2(\omega)$ of the dielectric function $\epsilon(\omega)$ in the random-phase approximation without allowance for local field effects can be calculated by summing all the possible transitions from the occupied and unoccupied states with fixed \mathbf{k} -vector over the Brillouin zone and is given as³⁴

$$\epsilon_2(\omega) = \frac{Ve^2}{2\pi\hbar m^2\omega^2} \int d^3k \sum |\langle \psi_C | p | \psi_V \rangle|^2 \delta(E_C - E_V - \hbar\omega) \quad (5)$$

Here, ψ_C and ψ_V are the wave functions in the conduction and

valence bands, p is the momentum operator, ω is the photon frequency, and \hbar is Planck's constant. The real part $\epsilon_1(\omega)$ of the dielectric function can be evaluated from $\epsilon_2(\omega)$ using the Kramer–Kroning relations.

$$\epsilon_1(\omega) = 1 + \frac{2}{\pi} P \int_0^\infty \frac{\epsilon_2(\omega') \omega' d\omega'}{(\omega')^2 - \omega^2} \quad (6)$$

where "P" is the principle value of the integral. The knowledge of both the real and imaginary parts of the dielectric function allows the calculation of the important optical properties such as refractive index, absorption, and photoconductivity.³⁴

In this present study, we investigated the static dielectric constant, refractive index, absorption spectrum, and photoconductivity of lithium azide along the three crystal directions at ambient pressure as well as at the high pressures. The static dielectric constant $\epsilon_1(0)$ as a function of pressure is shown in Figure 6a. Clearly $\epsilon_1(0)$ increases with pressure along all three directions. The static refractive index ($n = \epsilon^{1/2}(0)$) of the system in three directions is given by $n_{100} = 1.73$, $n_{010} = 1.34$, and $n_{001} = 2.61$. Clearly, $n_{100} \neq n_{010} \neq n_{001}$; therefore, we conclude that the lithium azide is an anisotropic crystal with biaxial crystal properties. At ambient pressure, our calculated values of $\epsilon_1(0)$ and $n(0)$ along the [100] direction are in good agreement with that of previous calculations.⁸ The calculated refractive index increases with an increase in pressure, as shown in Figure 6b, imply that the crystal binding will be more under the application of pressure. In Figure 6c, we have shown the calculated absorption spectra and photoconductivity spectra of LiN₃ along the [100], [010], and [001] directions at 0 GPa. Our calculated results indicate that there is anisotropy in the calculated optical spectra. Our calculated absorption spectra along the [100] direction are in good agreement with that of the reported absorption spectra in ref 8. The peaks in the absorption spectra are due to the interband transitions from the occupied to unoccupied states. The absorption starts from the energy of 3.32 eV, which is the energy gap between the valence and conduction bands. The first absorption peak in all three directions is observed at (5.98 eV), but the absorption coefficient is found to be different and it is around $1.9 \times 10^7 \text{ m}^{-1}$ in the [100] and [010] directions, whereas it is $4.5 \times 10^7 \text{ m}^{-1}$ along the [001] direction. From this result the decomposition of lithium azide takes place under the action of ultraviolet light that starts from the absorption edge of 3.32 eV.

Photoconductivity is due to the increase in the number of free carriers when photons are absorbed. The calculated photoconductivity shows that LiN₃ is photosensitive and displays a wide photocurrent response in the absorption region of 3.3–20 eV. The calculated absorption and photoconductivity spectra at pressures of 20, 40, and 60 GPa are shown in Figure 6d–f, respectively. It can be clearly observed that the fundamental absorption energy region and also the absorption coefficient along the three crystallographic directions increase with pressure. At 0 GPa, the fundamental absorption was found to be between 3.3 and 20 eV, and at 20 GPa, it increases to 23 eV and it further increases to 25 and 28 eV at 40 and 60 GPa. And also the absorption coefficient along the three directions increases with pressure over the entire absorption energy region. This means that as pressure increases, the response of the electrons to the incident photon energy increases. This can be understood by the increase in photoconductivity, which shows a broad photocurrent response in the absorption region as pressure increases. Overall, lithium azide shows a strong absorption (absorption

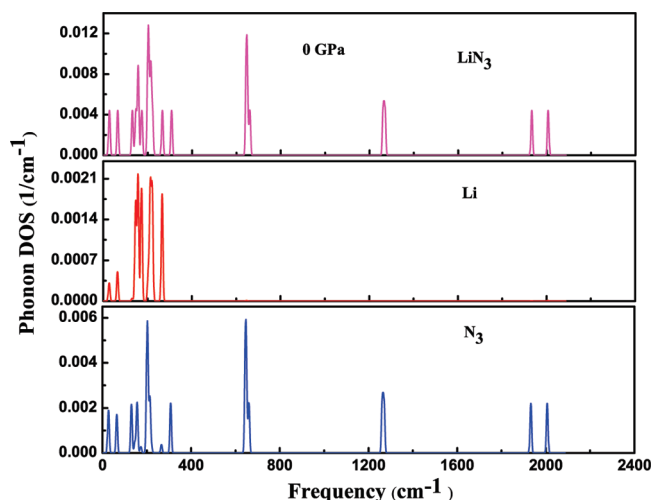


Figure 7. Total and partial phonon density of states (PhDOS) of LiN₃ at 0 GPa.

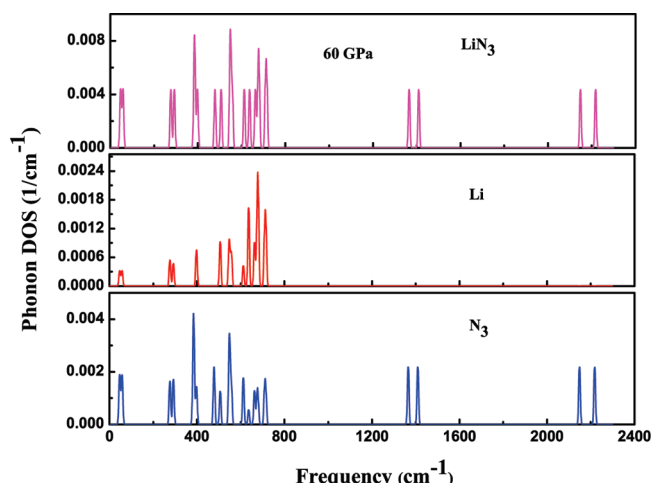


Figure 8. Total and partial phonon density of states (PhDOS) of LiN₃ at 60 GPa.

coefficient of the order of 10^7 m^{-1}) as a function of pressure over a broad energy range. Therefore from the study of optical properties of lithium azide under pressure we came to a conclusion that, although LiN₃ is stable up to 60 GPa, it may become unstable or decompose under the action of light which is equal to the absorption energy range of LiN₃ (ultraviolet light). In the above case LiN₃ becomes more unstable and decomposes easily into metal and nitrogen under pressure by the influence of ultraviolet light.

E. Vibrational Properties. Vibrational properties are obtained by the use of the linear response method within the density functional perturbation theory (DFPT).²³ In this method the force constants matrix can be obtained by differentiating the Hellmann–Feynman forces on atoms with respect to the ionic coordinates. This means that the force constant matrix depends on the ground-state electron charge density and on its linear response to a distortion of atomic positions. By variational principle the second-order change in energy depends on the first-order change in the electron density, and this can be obtained by minimizing the second-order perturbation in energy which gives the first-order changes in the density, wave functions, and potential. In the present study the dynamical matrix elements

Table 3. Calculated Vibrational Frequencies of Monoclinic LiN₃ at Ambient Pressure, Pressure Coefficients (cm⁻¹/GPa), and Grüneisen Parameters (γ) of the Vibrational Frequencies of All Vibrational Modes of Monoclinic LiN₃ from the Linear Fit of the Present GGA Results

mode	symmetry	frequency (cm ⁻¹)	pressure coefficient (cm ⁻¹ /GPa)	Grüneisen parameter (γ)
M1	B _u	138	2.1	1.26
M2	A _u	140.2	2.3	1.31
M3	A _u	143.4	3.4	1.54
M4	B _u	155.9	3.4	1.52
M5	A _u	172.5	3.1	1.40
M6	B _u	189.7	4.6	1.66
M7	B _g	191.6	4.9	1.68
M8	B _u	202.3	5.7	1.87
M9	B _u	210.1	5.5	1.79
M10	A _g	212.2	5.3	1.71
M11	B _u	220.7	6.2	1.84
M12	B _u	264.6	5.8	1.56
M13	A _g	304.6	8.1	1.53
M14	A _u	640.0 (635) ^a	0.5	0.04
M15	B _u	645.4	0.5	0.03
M16	A _u	645.6	1.1	0.14
M17	B _u	661.3	0.8	0.11
M18	A _g	1262.5	1.6	0.14
M19	A _g	1269.5 (1277) ^a	2.2	0.21
M20	B _u	1933.3	3.3	0.19
M21	B _u	2006.5 (2092) ^a	3.3	0.17

^aValues in parentheses are from experiment (ref 3).

are calculated on the $5 \times 8 \times 5$ grid of k -points using the linear response approach. The calculated total and partial phonon density of states of LiN₃ at 0 and 60 GPa are shown in Figure 7 and Figure 8. From the partial phonon density of states it can be observed that, at 0 GPa, the frequency modes below 300 cm⁻¹ are due to both the lithium and azide ion, whereas above this frequency the states are entirely dominated by the azide ion. At 60 GPa, the modes are shifting toward a high-frequency region.

The vibrational frequencies at Γ point are shown in Table 3. The group symmetry decomposition into irreducible representations of the C_{2/m} point group yields a sum of A_u + 2B_u for three acoustic modes and 4A_g + 2B_g + 5A_u + 10B_u for the 21 optical modes. The modes from M1 to M13 involve the vibrations from the lattice (including both metal atom and azide ion), whereas modes from M14 to M21 are entirely due to the azide ion. The M14 mode, which is due to the N₃ symmetric bending along *b*-axis, has a frequency of 640.02 cm⁻¹ and is in good agreement with that of the experimental value³ of 635 cm⁻¹. The M15 mode, located at 645.45 cm⁻¹, originates from the asymmetric bending of azide ion along the *b*-axis. The M16 and M17 modes having frequencies of 645.45 and 645.62 cm⁻¹ are due to the symmetric and asymmetric bending of azide ion along *a*-axis. The modes from M18 to M21 are the stretching modes of azide ion. Our calculated value of 1262.51 cm⁻¹ for the symmetric stretching of azide ion is in good agreement with that of the experimental value³ of 1277 cm⁻¹. The asymmetric stretching frequency of azide ion is found to be 2006.51 cm⁻¹, a value lower

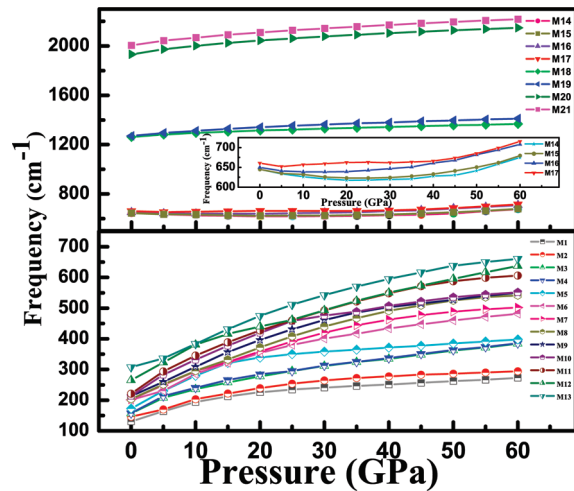


Figure 9. Pressure-induced shifts of vibrational frequencies of LiN₃. The inset shows the enlarged case of pressure dependence of M14 to M17 modes.

than that of the experimental value of 2092 cm⁻¹. This discrepancy may be due to the overestimation of the crystal volume because of GGA exchange-correlation functionals. To understand the intramolecular and intermolecular interactions under compression, we calculated the vibrational frequencies for the optimized crystal structures up to the pressure of 60 GPa at a pressure step of 5 GPa, which are shown in Figure 9. It can be clearly observed that as pressure increases, all of the vibrational frequencies of all modes from M1 to M21 increases, except the bending modes of azide ion from M14 to M17, which decrease and have minima at about 30 GPa for M14 and M15 modes, at about 10 GPa for M16 mode, and at 5 GPa for M17 mode. This clearly shows that the intramolecular interaction enhances under the application of pressure. In Table 3 we have shown the coefficients for the pressure-induced shifts of the vibrational frequencies of all vibrational modes of LiN₃ from M1 to M21. These values are obtained by a linear fit of the vibrational frequencies with respect to pressure. From the calculated values it is clear that different vibrational modes show distinctly different pressure-dependent behavior. The pressure coefficients for lattice modes are found to be higher than that of internal modes, indicating that the lattice modes show the most significant shift over internal modes. The lattice mode M13 has a high pressure coefficient of 8.1 cm⁻¹/GPa, and among the internal modes, the asymmetric stretching modes of azide ion M20 and M21 have a high pressure coefficient of 3.3 cm⁻¹/GPa. Overall the behavior of vibrational modes under compression indicates that the intermolecular and intramolecular interactions increase. The observed frequency shifts are more for lattice modes compared to the internal modes under compression. This implies that intermolecular interaction is affected more significantly than the intramolecular interaction under compression.

The knowledge of the volume dependencies of the vibrational modes allows one to calculate the Grüneisen parameters (γ_i) associated with them. The Grüneisen parameter of the *i*th vibrational mode can be defined as

$$\gamma_i = -\frac{\partial(\ln \nu_i)}{\partial(\ln V)} \quad (7)$$

The calculated γ_i of LiN₃ resulting from a linear fit of the ln ν as a function of ln V are listed in Table 3. It can be observed from

Table 3 that the calculated γ is high for lattice modes and the values are low for internal modes, which are entirely due to the azide ion vibrations. This also implies that the change in lattice parameters and thereby the volume with pressure has a large affect on vibrational modes, especially lattice modes, whereas the vibrational frequencies of azide ion have less influence by the pressure.

IV. CONCLUSIONS

In summary, the structural, electronic, optical, and vibrational properties of lithium azide under hydrostatic compression up to 60 GPa have been studied using density functional theory within generalized gradient approximation. The calculated structural parameters are overestimated compared to the experiment, which is due to the GGA exchange-correlation functionals. It is also observed that lithium azide remains in the monoclinic structure in the studied pressure range of 60 GPa as observed in experiment. From the calculation of total and partial DOS it is found that lithium azide is an ionic solid with a band gap of 3.32 eV and the gap decreases as pressure increases, indicating its ability to become semiconductor at high pressures. The single-crystal elastic constants at ambient pressure have been calculated, and it was found that the system is mechanically stable. The calculation of refractive index suggests that LiN₃ is an anisotropic material and the anisotropy increases with pressure. The absorption spectra and photoconductivity spectra at various pressures have been calculated, and it was found that the absorption peaks are shifting toward the high-energy region and photocurrent increases as pressure increases. Therefore we conclude that the decomposition of lithium azide is more favorable by the action of light (ultraviolet) under pressure. The vibrational frequencies at ambient and high pressures have been calculated.

At ambient pressure the calculated vibrational frequencies are in good agreement with the experiment values. The calculated vibrational frequencies at high pressures together with pressure coefficients and Grüneisen parameters show that the intermolecular interactions are highly affected by the applied pressure.

■ AUTHOR INFORMATION

Corresponding Author

*E-mail: gvsp@uohyd.ernet.in.

■ ACKNOWLEDGMENT

K.R.B. thanks DRDO through ACRHEM for financial support. All of the authors acknowledge CMSD, University of Hyderabad, for computational facilities.

■ REFERENCES

- (1) Fair, H. D.; Walker, R. F. *Energetic Materials*, Vol. 1; Plenum Press: New York, 1977.
- (2) Bowden, F. P.; Yoffe, A. D. *Fast Reactions in Solids*; Butterworth: London, U.K., 1958.
- (3) Evans, B. L.; Yoffe, A. D.; Gray, P. *Chem. Rev.* **1959**, *59*, 515.
- (4) Seel, M.; Kunz, A. B. *Int. J. Quantum Chem.* **1991**, *39*, 149.
- (5) Gordienko, A. B.; Zhuravlev, Y. N.; Poplavnoi, A. S. *Phys. Status Solidi B* **1996**, *198*, 707.
- (6) Gordienko, A. B.; Poplavnoi, A. S. *Phys. Status Solidi B* **1997**, *202*, 941.
- (7) Younk, E. H.; Kunz, A. B. *Int. J. Quantum Chem.* **1997**, *63*, 615.
- (8) Zhu, W.; Xiao, J.; Xiao, H. *Chem. Phys. Lett.* **2006**, *422*, 117.
- (9) Eremets, M. I.; Gavriliuk, A. G.; Trojan, I. A.; Dzivenko, D. A.; Boehler, R. *Nat. Mater.* **2004**, *3*, 558.
- (10) Eremets, M. I.; Hemley, R. J.; Mao, H. K.; Gregoryanz, E. *Nature* **2001**, *411*, 170.
- (11) Eremets, M. I.; Popov, M. Yu.; Trojan, I. A.; Denisov, V. N.; Boehler, R.; Hemley, R. J. *J. Chem. Phys.* **2004**, *120*, 10618.
- (12) Medvedev, S. A.; Trojan, I. A.; Eremets, M. I.; Palasyuk, T.; Klapötke, T. M.; Evers, J. *J. Phys.: Condens. Matter* **2009**, *21*, 195404.
- (13) Payne, M. C.; Teter, M. P.; Allan, D. C.; Arias, T. A.; Joannopoulos, J. D. *Rev. Mod. Phys.* **1992**, *64*, 1045.
- (14) Segall, M.; Lindan, P.; Probert, M.; Pickard, C.; Hasnip, P.; Clark, S.; Payne, M. *J. Phys.: Condens. Matter* **2002**, *14*, 271.
- (15) Vanderbilt, D. *Phys. Rev. B* **1990**, *41*, 7892.
- (16) Kresse, G.; Furthmüller, J. *Phys. Rev. B* **1996**, *54*, 11169.
- (17) Fischer, T. H.; Almofl, J. *J. Phys. Chem.* **1992**, *96*, 9768.
- (18) Ceperley, D. M.; Alder, B. J. *Phys. Rev. Lett.* **1980**, *45*, 566.
- (19) Perdew, J. P.; Zunger, A. *Phys. Rev. B* **1981**, *23*, 5048.
- (20) Perdew, J. P.; Burke, K.; Ernzerhof, M. *Phys. Rev. Lett.* **1996**, *77*, 3865.
- (21) Monkhorst, H. J.; Pack, J. *Phys. Rev. B* **1976**, *13*, 5188.
- (22) Pringle, G. E.; Noakers, D. E. *Acta Crystallogr.* **1968**, *24*, 262.
- (23) Gonze, X. *Phys. Rev. B* **1997**, *55*, 10337.
- (24) Refson, Keith.; Tulip, P. R.; Clark, S. J. *Phys. Rev. B* **2006**, *73*, 155114.
- (25) Mehl, M. J.; Osburn, J. E.; Papaconstantopoulos, D. A.; Klein, B. M. *Phys. Rev. B* **1990**, *41*, 10311.
- (26) Perger, W. F. *Int. J. Quantum Chem.* **2010**, *110*, 1916.
- (27) Perdew, J. P.; Chevary, J. A.; Vosko, S. H.; Jackson, K. A.; Pederson, M. R.; Singh, D. J.; Fiolhais, C. *Phys. Rev. B* **1992**, *46*, 6671.
- (28) Perdew, J. P.; Levy, M. *Phys. Rev. Lett.* **1983**, *51*, 1884–1887.
- (29) Jones, R. O.; Gunnarsson, O. *Rev. Mod. Phys.* **1989**, *61*, 689–746.
- (30) Manjon, F. J.; Errandonea, D.; Segura, A.; Munoz, V.; Tobias, G.; Ordejón, P.; Canadell, E. *Phys. Rev. B* **2001**, *63*, 125330.
- (31) Kanchana, V.; Vaiteeswaran, G.; Souvatzis, P.; Eriksson, O.; Lebègue, S. *J. Phys.: Condens. Matter* **2010**, *22*, 445402.
- (32) Bheema Lingam, Ch.; Ramesh Babu, K.; Tewari, S. P.; Vaiteeswaran, G.; Lebègue, S. *Phys. Status Solidi RRL* **2010**, *5* (1), 10.
- (33) Born, M.; Huang, K. *Dynamical Theory of Crystal Lattices*; Oxford University Press: Oxford, U.K., 1998.
- (34) Sinha, Sonali.; Sinha, T. P.; Mookerjee, A. *Phys. Rev. B* **2000**, *62* (13), 8828.